RMIT
UNIVERSITY

Thank you for downloading this document from the RMIT Research Repository.

The RMIT Research Repository is an open access database showcasing the research outputs of RMIT University researchers.

RMIT Research Repository: http://researchbank.rmit.edu.au/

PLEASE DO NOT REMOVE THIS PAGE

Interaction of laminate damage and adhesive disbonding in composite scarf joints subjected to combined in-plane loading and impact

M. K. Kim[1], D. J. Elder[2], C. H. Wang[1] and S. Feih[1,*]

[1]*School of Aerospace, Mechanical and Manufacturing Engineering, Royal Melbourne Institute of Technology, Bundoora, Victoria, 3083, Australia*

[2]*Cooperative Research Centre for Advanced Composite Structures, 506 Lorimer Street, Fishermans Bend, Victoria 3207, Australia*

---

[*] Corresponding author, stefanie.feih@rmit.edu.au

Abstract

Impact tests were carried out on composite laminates and composite scarf repairs, while both were subjected to in-plane loading with tensile pre-strain levels up to 5000 microstrain. The results show that pre-straining of the composite laminates has no noticeable influence on the size of the delamination area for the given impact energy of 8 J, which represents a typical barely-visible impact on thin-skin composite structures. For composite scarf joints, however, resulting damage has been found to be combination of adhesive disbonding and matrix cracking (delamination and intraply cracking) in the composite laminate. The size of this mixed type of damage increases significantly with increasing pre-strain levels. A finite element model was developed to investigate the interaction between adhesive disbonding and composite delamination. The computational results reveal that both delamination and adhesive disbonding are dominated by the mode II fracture. Since the critical mode II fracture energy release rate for composite laminates (G_{IIC}=1.08 kJ/m^2) is much less than that pertinent to the adhesive (G_{IIC}=3.73 kJ/m^2), delamination tends to occur first in the composite laminates, which then shield the growth of disbonding in the adhesive.

Keywords: composite, scarf joint, preload, dynamic impact, delamination

1. Introduction

The use of composite materials in primary aircraft structures is increasing significantly with the recent design changes in modern commercial aircraft. This increased application of composites gives rise to a heightened demand for composite repair technologies. Generally the scarf repair method is preferred over mechanical fastened repairs due to its superior structural efficiency and conformity to the external contour of the original structure [1-4].

Aircraft structures, and particularly external surfaces, are vulnerable to foreign object damage (FOD) while in service, during take-off, or landing. Despite the considerable studies devoted to the effect of dynamic impact damage on solid composite structures (references 5 and 6 present a good review), studies and models investigating the impact response of repaired composite structures while under load are currently lacking. Harman and Wang [1,2] investigated the structural efficiency of scarf repairs after impact, while the structure remained un-loaded. Baker *et al* [4] reported that a typical pre-tension strain level of military aircraft in service can reach 4000 ~ 5000 microstrain. So it is important to ensure that composite repairs are able to sustain the design loads in the event of impact damage while the structure is under load. In particular, it is vital to ensure that repairs are designed such that the impact damage while under load will not cause the residual strength to fall below the design limit loads. A combination of static pre-strain during dynamic impact events represents an extreme damage scenario, which should be considered in the design of scarf repairs.

Presently the design analysis of scarf repairs considers the loading capacity of the adhesive bond [2,3], without considering the influence of external impact while the repair is under load. Studies by Feih *et al* [7] and Li *et al* [8] indicated that scarf joints may suffer catastrophic failure under a combination of impact and pre-loading. However, it is not clear whether this type of failure is caused by damage in the composite laminates or in the adhesive bond. Impact loading on composite scarf repairs may cause matrix cracking and delamination in the composite laminate, as well as disbonding of the adhesive. Since structural adhesives are toughened to resist brittle fracture, they have higher fracture toughness but lower strength than the thermoset matrix (e.g., epoxy) in fibre composites [9-11]. The relative significance of these two properties on the load-carrying capacity of scarf repairs is not clear. This lack of

knowledge has hampered the development of design methodologies and tools for the design of scarf repairs to resist impact damage.

This paper studies the impact response of pre-loaded scarf joints. The interaction of composite delamination and bond line damage during impact under pre-strain is investigated through experimental testing and numerical analysis. To investigate the effects of impact energy and pre-strain levels on the damage tolerance of scarf joints, experimental testing and computational simulation are carried out for varying levels of both experimental parameters. The various failure modes, including adhesive failures inside the bond region, interfacial failure between adhesive and the composite adherend, and delamination in the laminates, are investigated with respect to pre-strain and impact levels. Results are compared to numerical predictions. Bond line damage is identified as the main failure mode controlling joint strength following impact. A cohesive failure approach is employed to model and predict the failure of the bond line region and ply delamination as a function of impact parameters. The presented research findings pave the way for the development of a design methodology for scarf joint repairs in primary structures under pre-load, which are exposed to a possible foreign object impact damage event.

2. Materials and Testing

2.1 Composite Laminates and Scarf Joints

Aerospace grade Cycom 970/T300 unidirectional prepreg was used for the composite coupons and composite scarf joint adherends. A quasi-isotropic lay-up of $[45/90/-45/0]_{2S}$ was chosen, resulting in a total thickness of 3.2 mm. Following autoclave cure at 180°C and positive pressure of 690 kPa, composite laminates with a width of 100 mm were bevelled to a scarf angle of 5° and bonded with Cytec FM 300 film adhesive, representing a hard-patch method repair method. Cytec FM300 film adhesive is a rubber-toughened epoxy adhesive and extensively used in F/A-18 aircraft for bonding composite skins to honeycomb core [12,13]. The bond line had a thickness of 0.38 mm and a bond line length of 36.7 mm due to the small scarf angle, resulting in a total adhesive area of 3670 mm^2.

2.2 Impactor Conditions

Figure 1 shows a schematic of the impact test set-up with pre-strain. The unsupported specimen length and width are 140 and 100 mm, respectively. The impact point is located at the centre of the test specimen. The test fixture applies a constant tensile strain during the impact event.

In order to represent the low-weight and high-velocity impact conditions pertinent to runway debris [14], a composite lightweight impactor with a mass of m_I=410 g was designed. The impactor consists of a main composite body, rail guards made of Teflon and a steel impactor tub with a diameter of 12 mm. The impactor force was captured by a 5kN force transducer (PCB Model 240), located between the rigid impactor tub (m_R=70g) and the main composite body (m_{comp}=340g). The measured contact force, F_{FT}, was corrected by the mass ratio of impactor body and impactor in order to report the tip contact forces, $F_{contact}$ [15]:

$$F_{contact} = F_{FT}\left(1 + \frac{m_R}{m_{comp}}\right)$$
(1)

Inbound velocities were determined for each test to establish the impact energy:

$$E_{impact} = \frac{1}{2}m_I v^2$$
(2)

Laminate coupons and scarf joints were tested at different pre-strain levels and two different impact energies (2 Joules and 8 Joules). The lower impact energy of 2 Joules determines the elastic response as a function of pre-strain. At the higher impact energy of 8 Joules, catastrophic failure for the scarf joints occurred at a pre-strain level of 4000 microstrain.

2.3 Non-destructive damage evaluation

All tested specimens were scanned from both sides using ultrasonic C-scanning following the impact event to characterise the area of the damage region. Additionally, selected specimens were sectioned to establish a detailed damage profile through-the-thickness using a Leitz microscope with digital camera attachment.

3. Numerical Approach

3.1 Finite element model

A finite element model was developed using Abaqus v6.9 [16]. A two-step modelling approach with static pre-strain followed by the impact was employed, and the problem was analysed using the Abaqus/Explicit solver. The impactor was modelled as an analytical (rigid) surface to minimise discretisation errors and computational time.

Three-dimensional solid elements were employed to accurately model the adherend lay-up around the bond line of the scarf joint region; the mesh is presented in Figure 2. Except for an interfacial region where six-node solid elements (C3D6R) were used to avoid low quality of element shape (such as high aspect ratio or skew), eight-noded solid elements (C3D8R) with reduced integration were adopted to minimise computational time and to avoid shear locking. The default hourglass control was used for these elements [16]. Convergence studies for peak force and maximum deflection were undertaken to ensure that the mesh was adequate, and the hourglassing energy was less than 1% of the internal energy [15]. Each layer of solid elements represents one composite ply, i.e. there are 16 layers of elements through the laminate thickness. The ply-by-ply technique enhances the ability to account for the through-thickness transverse loading effect (or bending effect). Table 1 summarises the material data used for the composite adherends as determined based on manufacturer's data and tensile and bending tests according to ASTM D3039 and D790-02, respectively [15]. The properties are within 10 - 20% of values specified by the composite prepreg manufacturer.

4.2 Delamination and bond line modelling

Both delamination and bond line damage need to be captured in the analysis. For delamination damage, surface-based cohesive behaviour [16] was prescribed at all ply interfaces. For the adhesive bond region, eight-noded cohesive elements (COH3D8) were adopted due to the finite thickness of the adhesive layer. The arrows in Figure 2 indicate the stacking direction for the traction-separation law. Due to the relatively thin bond line, a mesh with non-matching nodes is required. Mismatching nodes on the adherend and the adhesive surfaces were tied using the Abaqus tie constraint [16].

For both adhesive and delamination damage modelling, the bilinear traction-separation was adopted for damage initiation and damage evaluation. The damage initiation was modelled as a quadratic stress interaction relationship:

$$\left(\frac{\sigma_{11}}{\sigma_{ult,1}}\right)^2 + \left(\frac{\tau_{12}}{\sigma_{ult,2}}\right)^2 + \left(\frac{\tau_{13}}{\sigma_{ult,3}}\right)^2 = 1, \tag{3}$$

where σ_{11}, τ_{12} and τ_{13} refer to the normal stress, the in-plane stress, and the transverse shear stress in the cohesive layer. The respective ultimate strength values are denoted by parameters $\sigma_{ult,1}$, $\sigma_{ult,2}$, and $\sigma_{ult,3}$.

The damage evolution was based on fracture energy criterion which is defined as below:

$$e_d = \left(\frac{G_I}{G_{IC}}\right)^\alpha + \left(\frac{G_{II}}{G_{IIC}}\right)^\alpha + \left(\frac{G_{III}}{G_{IIIC}}\right)^\alpha \le 1 \tag{4}$$

where G_I denotes the fracture toughness in normal mode, G_{II} the in-plane shear, and G_{III} the transverse shear. The subscript "c" denotes the critical fracture energy in each mode. The extent of accounting for mixed-mode effects can be determined by the exponential parameter α, based on the power law approach. In the present investigation, the parameter α is set to have a fixed value of unity. If the scalar damage, e_d, is less than unity, the material is assumed to be intact. Upon reaching $e_d = 1$, the cohesive element is considered to have failed. In the current study the failed elements were deleted from the analysis for both delamination and adhesive failure modes [16]. The area of the deleted elements gives the damage area, which will then be compared with the experimental results from C-scan measurements.

In the present investigation, we will limit our attention to strain-rate independent analysis. Table 2 summarises the material parameters for the cohesive failure behaviour. The values for delamination failure are based on numerical results by Pinho *et al* [17] for the carbon composite T300/913 prepreg system. The strength and fracture toughness values for the adhesive are taken from the static data by the manufacturer [4,12]. The adhesive stiffness is generally considered independent of rate-effects and was considered constant [10,11]. Previous investigations have indicated that the fracture behaviour of rubber-modified epoxies is visco-elastic, giving rise to strong rate effects [9] at very high strain rate. Strength has generally been shown to increase under dynamic conditions for rubber-toughened epoxies as

the material becomes less ductile, because there is insufficient time to respond to stress during visco-elastic deformation [18]. The size of the plastic zone is consequently decreased, and the adhesive will behave in a manner similar to that of a pure epoxy [19]. An upper limit for the dynamic strength based on the static strength was estimated as indicated in Table 2, but the sensitivity with respect to this value is shown to be weak in the following results section. The mode II fracture toughness, on the other hand, was found to be critical for the analysis problem as the scarf joint bond line fails predominantly under shear loading. The value was calibrated for the impact condition of $1000\mu\varepsilon$ tensile pre-strain. Computational studies reveal that the power law parameter α has a very weak effect on the predicted damage size, due to the dominance of the shear loading during the failure process. The static mode I fracture toughness was used in the current studies due to the weak dependence of results on this value.

4. Experimental and Computational Results

4.1 Elastic Response

It was found that the specimens subjected to impact energy of less than 4.5 Joules showed no damage in either adherend or adhesive region, up to a pre-strain level of $5000\mu\varepsilon$. The impact response for both laminates and scarfed specimens was found to be identical considering experimental result variation, thereby validating that the thin bond line of the scarf joint does not influence the elastic properties during elastic bending. This was also confirmed through numerical simulation for both laminates and scarf joints. Figure 3 shows the comparison of laminate and scarf joint response, together with the predicted numerical response. The impact duration is around 3ms, with multiple force peaks recorded during the impact event. The chosen modelling approach utilising the material parameters in Table 1 and Table 2 is shown to lead to good predictions for the elastic impact response.

4.2 Delamination Damage in Composite Coupons

Specimens subjected to 8 Joules impact energy sustained significant delamination damage and matrix cracking as shown by micrographs of polished specimens. Figure 4 shows the damage size as a function of pre-strain for the constant impact energy of 8 Joules. Two representative damage shapes are also indicated in this figure. The experimental damage predominantly consists of delamination up to $3000\mu\varepsilon$, with some matrix cracking across plies as determined by C-scanning. Delamination is detected between most interfaces, but more

severe towards the bottom ply interfaces. The damage is generally symmetrical around the impact centre. At the highest tested pre-strain level of 4000$\mu\varepsilon$, the damage area is no longer circular as ply splitting along the fibres occurred due to tensile bending strains in the lower external 45° surface ply. However, considering delamination damage only as indicated in the damage area figure, the damage area for the laminate is found to be independent of the applied pre-strain level (A_{dam}=180-200mm^2). Figure 4 also shows a comparison of the delamination area for experimental and numerical results as a function of varying pre-strain. The comparison results in two conclusions: (1) The results are in a good correlation except for the zero pre-strain level, therefore validating the modelling methodology and the cohesive material parameters for the delamination model; and (2) the numerical delamination size is confirmed to be independent of the pre-strain level for a given impact energy. It should be noted that other composite damage modes apart from delamination were not considered in the numerical analysis due to the chosen 3D modelling approach.

4.3 Adhesive Damage in Scarf Joints

Figure 5 shows the results from the C-scanning for an impact tested scarf joint at 8 Joules and 3000$\mu\varepsilon$. Different colours present the representative thickness of the detected damage. A circular damage pattern towards the upper surface can be distinguished from a lower damage pattern extending to the left side along the bond line. This damage pattern is significantly different from the circular damage pattern observed for the composite coupons, which is attributed to the additional development of adhesive damage in the bond line during impact. C-sectioning of the damage area in Figure 6 shows that an interaction of both adhesive and composite delamination takes place at higher pre-strain levels, as expected based on the overall damage shape. Cohesive failure occurs as cracks propagate along the bond line towards the bottom surface of the scarf joint (tensile side), which is consistent with C-scanning results in Figure 5. As for the composite laminates, both delamination and matrix cracking are found to occur in the composite adherends. The identified failure modes are very similar to failure modes in scarf joints tested with zero pre-strain, which were described by Harman and Wang [20] and Takahashi et al. [21]. It is observed that similar types of failure were found in all scarf joint irrespective of impact conditions. However, failure in the adhesive region and along the bond line was more pronounced for higher pre-strain levels.

Preliminary numerical results showed that the size of the adhesive damage area is most sensitive to changes in the mode II fracture toughness of the adhesive. This was expected due to the bending deformation during impact and resulting high shear stresses in the adhesive, which increase with increasing pre-strain. Peel stresses are minimised in scarf joint bond lines when compared to other joint types [3]. The impact result for a tensile pre-strain of $1000\mu\varepsilon$ was used to calibrate the mode II fracture toughness for the adhesive. This test case resulted in a total damage area of $250mm^2$, which is significantly higher than the corresponding laminate damage area of $200mm^2$ due to delamination only. Figure 7(a) indicates the sensitivity of the predicted total damage area with respect to the mode II fracture toughness for the adhesive and the ultimate shear strength. The predicted damage area increases nonlinearly with a decrease in fracture toughness, but predictions are mostly independent of the shear strength for the given fracture toughness range. This indicates that the fracture process is propagation-controlled rather than initiation-controlled. Figure 7(a) shows that a fitted value of $G_{IIC, adh} = 3.7$ N/mm is obtained when comparing the experimental damage area to the numerically predicted total damage area. This calibrated dynamic fracture toughness value for mode II is slightly larger than the estimated static value of $G_{IIC, adh} = 3.3$ N/mm as obtained from the area under the static shear stress-strain curve [4]. Figure 7(b) indicates the respective areas of delamination damage and adhesive damage as a function of adhesive fracture toughness. As expected, the influence of the adhesive fracture toughness on the composite delamination area is small in comparison to the changes in the adhesive damage area. At this pre-strain level, for the range of fracture toughness values investigated, the adhesive damage area remains significantly smaller than the delamination area.

Figure 8(a) shows the damage area as a function of pre-strain for the scarf joints at an impact energy of 8 Joules in comparison to the experimental results. While the damage area for the composite scarf joint coincides with respect to shape and size with the laminate for low pre-strain levels (delamination dominated), it increases significantly with an increase in pre-strain and becomes adhesive dominated. The damage shape changes significantly as the adhesive damage increases as indicated by C-scanning. Complete disbonding of the bond line occurred for one of three tested joints at $4000\mu\varepsilon$. The numerical predictions with the fitted fracture toughness of $G_{IIC, adh}=3.73$ N/mm capture this behaviour well up to $3000\mu\varepsilon$ and predict complete disbonding at a pre-strain level of $4000\mu\varepsilon$. Figure 8(b) shows the numerical contribution of adhesive to composite damage for varying pre-strain levels. As in the case of

the composite laminates, the amount of composite damage is mostly insensitive to the pre-strain level. The adhesive damage, on the other hand, increases linearly up to a pre-strain level of 3000 microstrain, followed by catastrophic damage at 4000 microstrain. This numerical result validates the experimental sensitivity of the adhesive damage area with respect to tensile pre-strain.

5. Discussion of Results

5.1 Influence of pre-strain on damage development

Figure 9(a) and (b) show the recorded force-time history graphs for both the composite laminate and the scarf joint at identical impact conditions at 8 Joules and 1000 $\mu\varepsilon$ and 3000 $\mu\varepsilon$. The increase in impact energy from 2 Joules (see Figure 3) to 8 Joules results in significantly higher peak forces during impact. The force-time response is shown to be similar for the laminate and scarf joints. For a given impact energy, it can be seen that the peak force for both laminate and scarf joint is only weakly dependent on the pre-strain level and is insensitive to the presence or damage of the scarf bond line. It is therefore reasonable to assume that the peak impact load is approximately constant, which enables a simple quasi-static analysis to estimate the shear stress distribution through the thickness of a scarf joint for various pre-strain levels. The shear stress is the main driving force for damage development (for both delamination and bond line damage) as discussed.

Let us consider the scarf joint, shown in Figure 10, which is subject to a combination of in-plane preloading and an impact load. The interlaminar shear stress τ_{xz} due to impact load (the coordinate system is shown in Figure 10) can be expressed in terms of the peak impact force [22],

$$\tau_{xz} = \frac{3P_{max}}{2t}\left[1 - \left(\frac{z}{t/2}\right)^2\right] \tag{5}$$

where P_{max} denotes the peak impact force, and t the thickness of the laminate. The interlaminar shear stress attains its maximum value at the mid-plane of the laminate. It is important to note that the pre-strain does not affect the interlaminar shear stress, and hence will have negligible effect on the size or area of delamination damage in the composite adherend, consistent with the experimental and numerical results presented in Figure 4 and Figure 8.

For the adhesively bonded scarf joint, the shear stress acting on the adhesive is caused by two loads: the shear stress given by equation (5), and the membrane stress resulting from the pre-straining and the bending moment due to the impact force. Using the rigid-bond analysis technique [3], the total shear stress in the coordinate system $x_1 z_1$ (referring to Figure 10) along the bond line is,

$$\tau_{x_1 z_1} = \left(\frac{\sigma_{applied}}{2} - \frac{P_{max}}{4} \right) \frac{L}{2} - x_1 \cos \alpha \left[\frac{z_1 \cos \alpha}{I} \right] \sin 2\alpha + \frac{3 P_{max}}{2t} \left[1 - \left(\frac{z_1 \cos \alpha}{t/2} \right)^2 \right] \cos 2\alpha \qquad (6)$$

where I denotes the bending stiffness of the laminate per unit width, which is equal to $t^3/12$. applied stress, $\sigma_{applied}$, is equal to the product of the in-plane laminate stiffness and the pre-strain, $i.e.$, $\sigma_{applied} = E_{lax\,min\,ate} \varepsilon_{pre-strain}$.

For the various combinations of pre-strain and impact loading considered in the present investigation, the adhesive shear stress is dominated by the first term and the third term in equation (6). This suggests that adhesive disbonding tends to occur at the centre of the joint, consistent with the experimental observations and the computational simulation. It is clear from the solution given in Equation (6) that the adhesive shear stress increases linearly with the pre-strain, suggesting that disbonding size will increase linearly with pre-strain. This is consistent with the results presented in Figure 8(b) up to the pre-strain of 3000 microstrain. Catastrophic damage occurs at 4000 microstrain due to the significant increase of the applied stress in the intact portion of the adhesive layer and cannot be predicted based on Eq. (6).

5.2 Sequence of Composite and Adhesive Failure

The sequence of failure events can be directly studied by comparison of the numerical results for the two failure events during the impact event, which is shown in Fig. 11. The numerical force-time history contains multiple equal-strength peak forces, which are not seen in the tests. This is most likely due to neglecting the in-plane composite failure modes. However, the numerical prediction was able to capture the accurate impact response as the initial stiffness gradient was similar and the first peak force is well matched.

When comparing the numerical and experimental results in (c) and (d) and the indicated failure event sequence, it can be seen that delamination is initiated early during the impact event and prior to adhesive damage; this failure sequence is independent of the applied tensile pre-strain. Damage development stopped once the last peak force value was reached.

5.3 Effects of combined adhesive and composite damage

The effects of simultaneous damage development for the composite and the adhesive were investigated numerically for an impact energy of 8 Joules and a tensile pre-strain of 1000 $\mu\varepsilon$. Three scenarios were investigated for this specific case:

- Composite damage only
- Adhesive damage only
- Combined composite and adhesive damage

Figure 12 compares the damage plots for the different damage scenarios. Figure 12(a) shows the damage in the adhesive layer, with total failure indicated by the deleted elements. An adhesive damage area of 100 mm^2 is predicted. Figure 12(b) shows the equivalent damage pattern if only composite damage is considered, which results in a composite damage area of 260mm^2. Combining both failure events reduces both composite and adhesive damage areas when considered separately, while the combined damage area is compared to the experimental C-scanning results. This is shown in Figure 12(c). Figure 12(d) indicates the distribution of the composite delamination through the thickness of the scarf joint. It can be seen that the delamination damage occurs above and below the adhesive bond line and intersects with the adhesive bond line damage. Table 3 summarises the damage areas for the different scenarios. The adhesive damage area reduces significantly by nearly 50% (reduction from 100 mm^2 to 57 mm^2) when both damage mechanisms are present. The composite damage area reduces only slightly, as this failure process is dominant and develops first. The mode II fracture energy of the composite is significantly lower, thereby giving preference to the development of delamination/disbonding between plies.

The preference of delamination damage during impact of bonded scarf joints is a significant finding as the catastrophic damage of the scarf joint occurs by adhesive disbonding. The

presence of the secondary composite damage mechanism reduces the area of adhesive damage due to the additional damage energy uptake when creating ply disbonding. This is indicated in Table 4 for different pre-strain values. The table compares the size of the adhesive damage area with and without delamination. Catastrophic failure is delayed significantly from approximately 2500με to 4000με when composite damage is included in the numerical model. The failure mode of composite delamination thereby effectively increases the required impact energy or velocity of an object to cause catastrophic failure of the joint for a given pre-strain value.

6. Conclusions

Based on the results of the experimental testing, computational simulation, and theoretical analysis presented in this paper, we can conclude the following:

1. Force-time histories are insensitive to the bond line presence and adhesive damage.

2. Pre-strain has negligible effect on the delamination size in composite laminates as confirmed through analytical and numerical analysis.

3. The area of disbonding in the bond line region of the scarf joint initially increases almost linearly with pre-strain, followed by catastrophic joint failure.

4. Delamination in composite laminates has been found to reduce the size of adhesive disbonding, partly due to the energy dissipation accompanying the delamination damage.

5. Cohesive zone modelling by incorporating separate traction laws for the adhesive disbonding and the composite delamination has been found to produce predictions in good correlation with the experimental results.

References

1. Harman AB and Wang CH. Damage tolerance and impact resistance of composite scarf joints. In: Proceedings of the 16th International Conference on Composite Materials (ICCM-16), Kyoto, 8-13 July 2007.

2. Harman AB and Wang CH. Improved design methods for scarf repairs to highly strained composite aircraft structure. Composite Structures 2006; 75(1-4): 132-144.

3. Wang CH and Gunnion AJ. On the design methodology of scarf repairs to composite laminates. Composites Science and Technology 2008; 68(1): 35-46.

4. Baker AA, Dutton S and Kelly DW. Composite materials for aircraft structures. AIAA Education Series, 2004.

5. Abrate S. Impact on composite structures. Cambridge University Press, 1998.

6. Hancox NL. An overview of the impact behaviour of fibre-reinforced composites. In: Reid SR and Zhou G., editors. Impact behaviour of fibre-reinforced composite materials and structures. CRC Press, Woodhead Publishing Ltd, 2000. p. 1-32.

7. Feih S, Gunnion AJ, Li HCH and Herszberg, I. Loaded carbon composite scarf joints subjected to impact, In: Proceedings of the 5th Australasian Congress on Applied Mechanics (ACAM 2007), Brisbane, 10 -12 December 2007.

8. Li H.C.H., Feih S., Gunnion A.J. and Herszberg I. Loaded carbon composite scarf joints subject to impact. In: Proceedings of the 14th International Conference on Composite Structures (ICCS14), Melbourne, 19-21 November 2007.

9. Hunston DL and Bullman GW. Visco-elastic fracture behaviour for different rubber-modified epoxy adhesive formulations. International Journal of Adhesion and Adhesives 1985; 5(2): 69-74.

10. Kinloch AJ, Shaw SJ, Tod DA and Hunston DL. Deformation and fracture behaviour of a rubber-toughened epoxy: 1. Microstructure and fracture studies. Polymer 1983; 24(10): 1341-1354.

11. Yee AF and Pearson RA. Toughening mechanisms in elastomer-modified epoxies. Journal of Materials Science 1986; 21(7): 2462-2474.

12. Cytec, FM300-2, Dual-cure capable film adhesive/surfacing film, 2007, Cytec Engineering materials: Havre de Grace, p. 1-4.

13. Charon A. Hot/Wet Environmental Degradation of Honeycomb Sandwich Structure Representative of F/A-18: Discolouration of Cytec FM-300 adhesive. Airframes and Engines Division, Aeronautical and Maritime Research Laboratory, DSTO-TN-0263, 2000

14. Cantwell WJ and Morton J. The impact resistance of composite materials. Composites 1991; 22(5): 347-362

15. Kim MK. Impact response of composite scarf joints under load. Master of Engineering Thesis, School of Aerospace, Mechanical and Manufacturing Engineering, RMIT University, 2010.

16. Abaqus Version 6.9 Documentation, 2009, Abaqus, Inc., Rhode Island, USA

17. Pinho ST. Modelling failure of laminated composites using physically-based failure models. PhD thesis, Department of Aeronautics, Imperial College London, UK, 2005.

18. Crocombe AD. Modelling and predicting the effects of test speed on the strength of joints made with FM73 adhesive. International Journal of Adhesion and Adhesives 1995, 15(1): 21–27.

19. Yamamoto I, Higashihara T and Kobayashi T. Effect of silica-particle characteristics on impact/usual fatigue properties and evaluation of mechanical characteristics of silica-particle epoxy resins. The Japan Society of Mechanical Engineers Part A 2003; 46(2): 145–153.

20. Harman AB and Wang CH. Analytic and finite element stress predictions in two-dimensional scarf joints. In: 11th Australian International Aerospace Congress (AIAC11), Melbourne, 15 – 17 March 2005.

21. Takahashi I, Takeda S, Iwahori Y and Takeda N. Evaluation of the impact damages of scarf-repaired composites. Journal of the Society of Materials Science 2007; 56(5): 414-419.

22. Timoshenko, S.P. and J.N. Goodier, Theory of Elasticity. 1970: McGraw-Hill.

Table 1: Static material properties for composite plies and adhesive layer

Material Property	Composite	Adhesive
E_1 [GPa]	96	2.4
$E_2=E_3$ [GPa]	6.4	2.4
$G_{12}=G_{13}$ [GPa]	4	0.9
G_{23} [GPa]	2.1	0.9
$\nu_{12} = \nu_{13}$	0.45	0.3
ν_{23}	0.2	0.3

Table 2: Mechanical properties used for adhesive failure and delamination modelling

Material Property	Delamination (after [17])	Adhesive (static)	Adhesive (dynamic)
K_I [N/mm^3]	1600000◊	6200[†]	6200[†]
$K_{II}=K_{III}$ [N/mm^3]	1600000	6200[†]	6200[†]
G_I [N/mm]	0.258	1.3[#]	Unknown
$G_{II}=G_{III}$ [N/mm]	1.08	3.2[#]	3.73[*]
α	1.21	1	1
$\sigma_{ult,\ 1}$ [MPa]	69.2	52.1[#]	~73.1[$]
$\tau_{ult,\ 2}=\tau_{ult,\ 3}$ [MPa]	40.0	30.1[#]	~52.0[$]
Density [Mg/mm^2]	1.5E-9	1.28E-9	1.28E-9

◊ High stiffness to ensure elastic response without softening due to multiple ply interfaces

[†] From material properties in Table 1 and adhesive layer thickness

[#] From static manufacturer's data and Baker *et al* [4].

*Fitted to produce best result for 8J and 1000με (see Figure 7)

[$] Estimated upper limit based on static strength

Table 3: Comparison of damage areas for different damage scenarios

Damage Case	Delamination area (mm^2)	Adhesive damage area (mm^2)	Total damage area (mm^2)
Delamination only	258		258
Adhesive damage only		99	99
Combined damage	235	57	248

Table 4: Comparison of damage areas for different pre-strain values

Tensile Pre-strain	Adhesive damage area without delamination (mm^2)	Adhesive damage area with delamination (mm^2)
0	41	38
1000	90	60
2000	1090	134
3000	Failed	194
4000	Failed	Failed

Figure 1: Schematic of impact test set-up
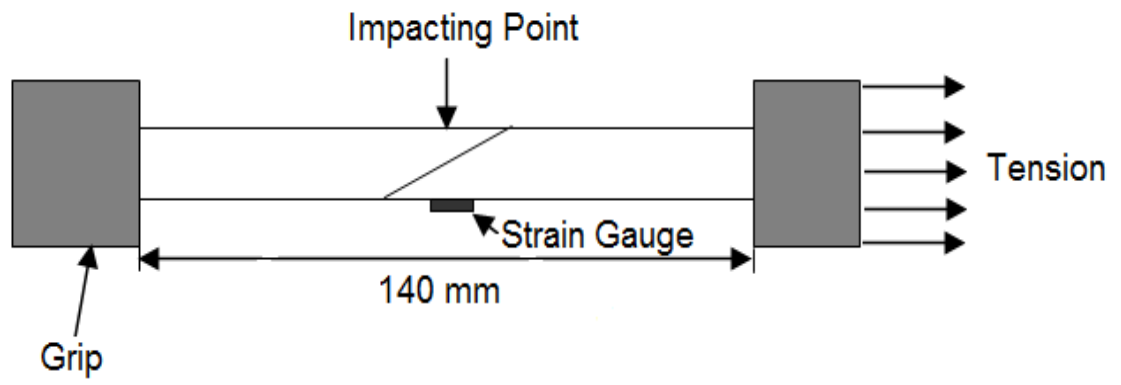
Figure 2: Schematic of scarf joint mesh with symmetric composite lay-up with *Tie constraints between mismatched nodes of the adhesive layer and composite plies. This approach allows for a higher mesh density of the cohesive layer.
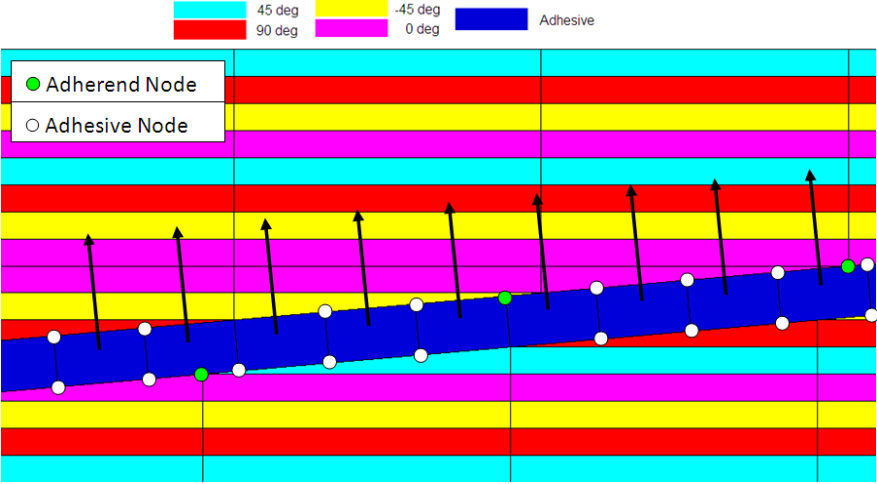
Figure 3: Force-time history at 2J at 1000με for elastic response validation. Scarf joint and composite laminate show the same characteristic response.
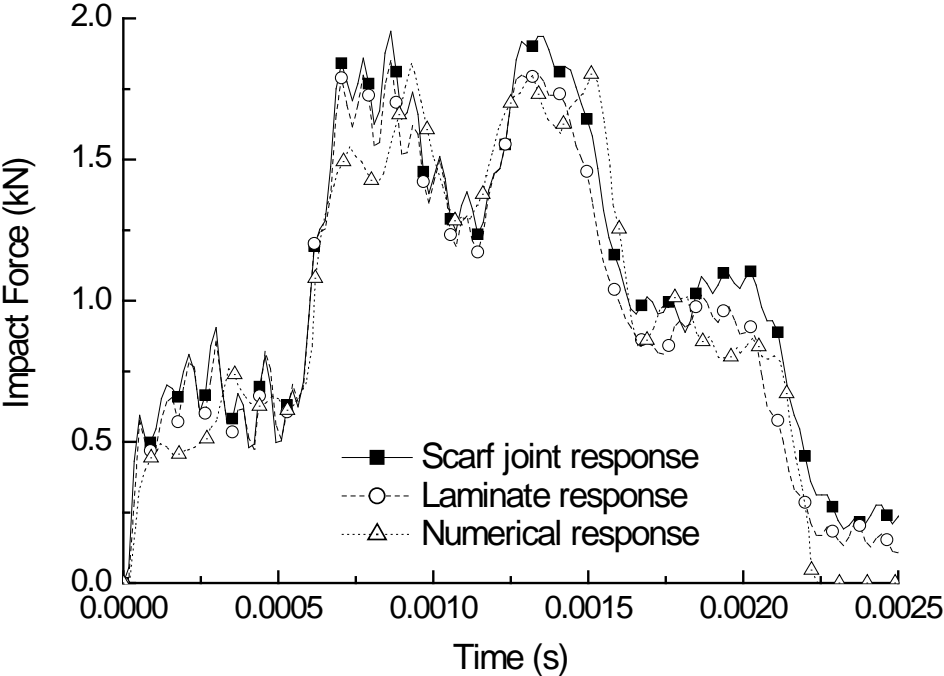
Figure 4: Delamination damage area versus pre-strain for composite laminates at an impact energy of 8J with various levels of pre-strain. Some experimental variation is due to differences in impact energy ($E_{imp} = 7.6 \pm 0.3$). Finite element results indicate no influence of pre-strain on delamination area.
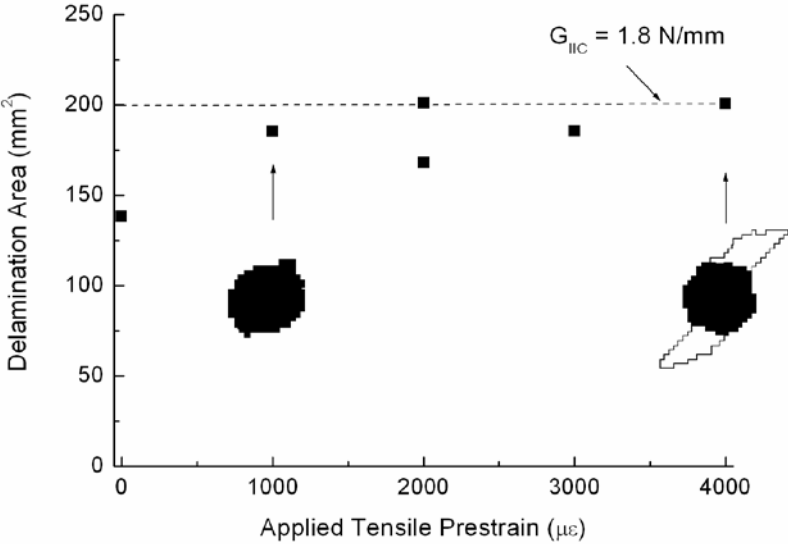
Figure 5: C-scanning damage area for an impact energy of 8J and a tensile pre-strain of 3000με.
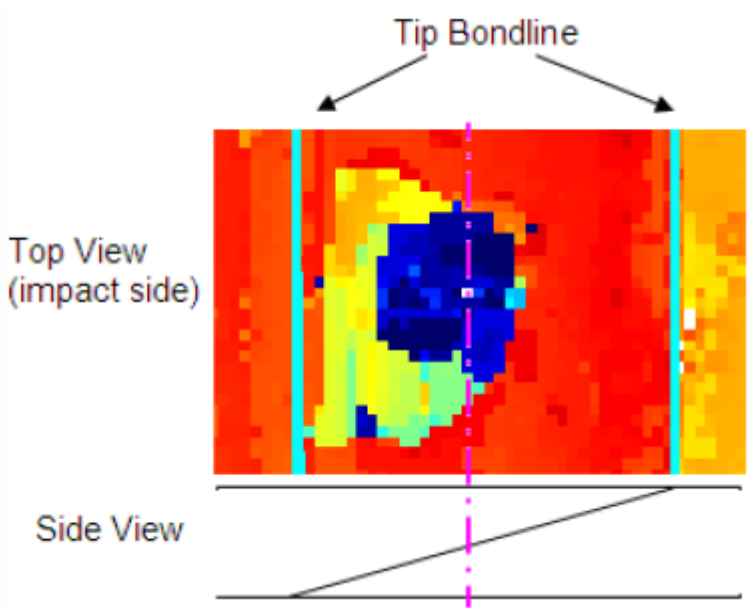
Figure 6: Damage pattern around the adhesive bond line for an impact energy of 8J and tensile pre-strain of 2000με.
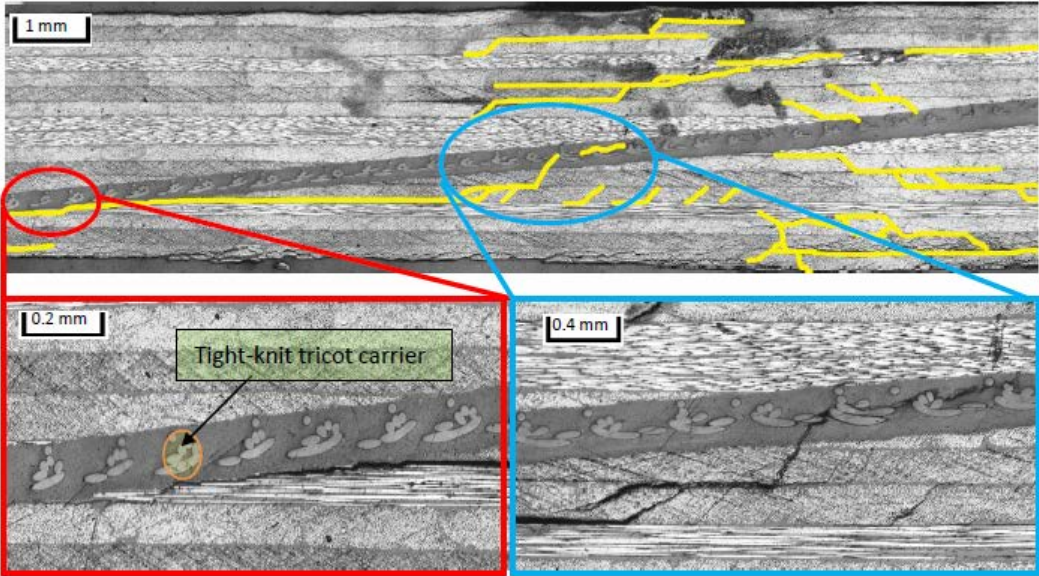
Figure 7: (a) Fitting of the mode II fracture toughness for the adhesive ($G_{IIC, adh}$=3.73 N/mm) with respect to the adhesive damage area at an impact energy of 8J and a tensile pre-strain of 1000$\mu\varepsilon$ for two ultimate stress values of 30 and 43 MPa. (b) The prediction of the composite damage area is shown to be insensitive to variations of the mode II adhesive fracture toughness.
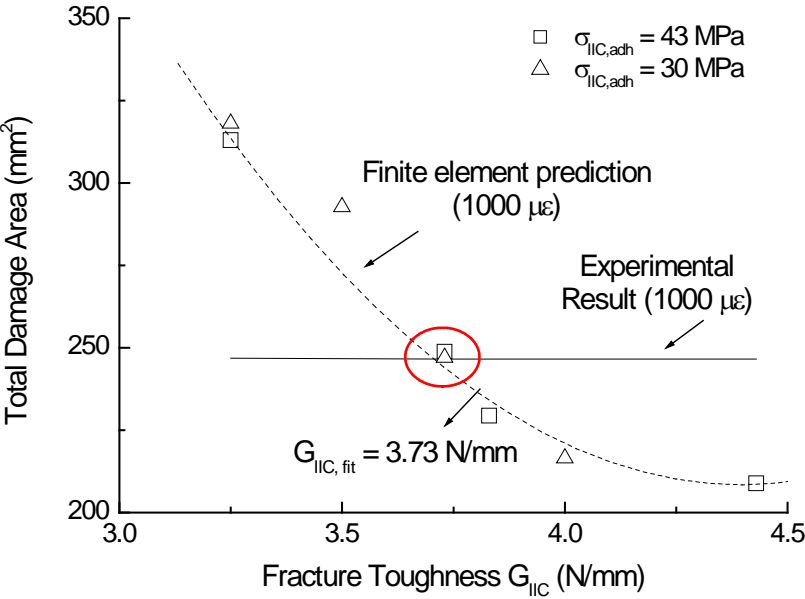
(a)
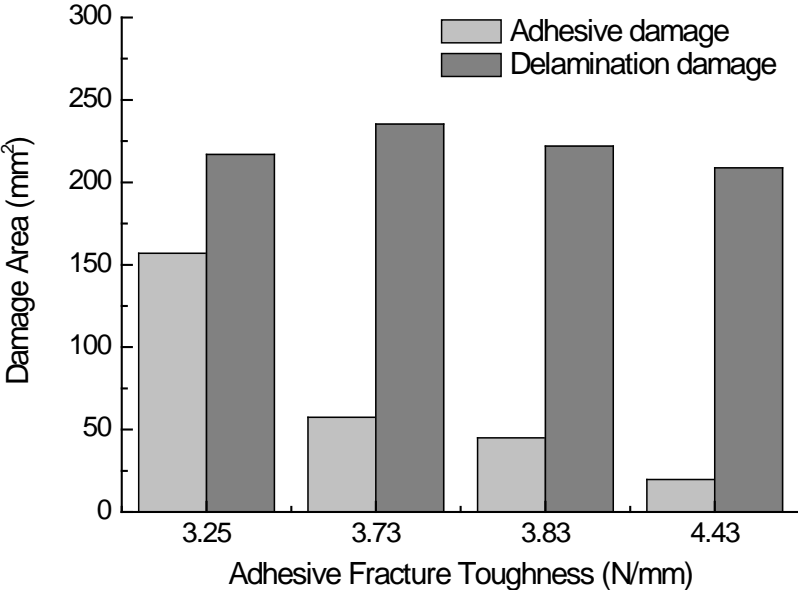
(b)

Figure 8: (a) Comparison of scarf joint and composite damage area and (b) contributions of composite and adhesive damage to total damage area. Finite element results are predicted with a fracture toughness of G_{IIC} = 3.73 N/mm. The value for the fracture toughness was fitted at a tensile pre-strain of 3000$\mu\varepsilon$.
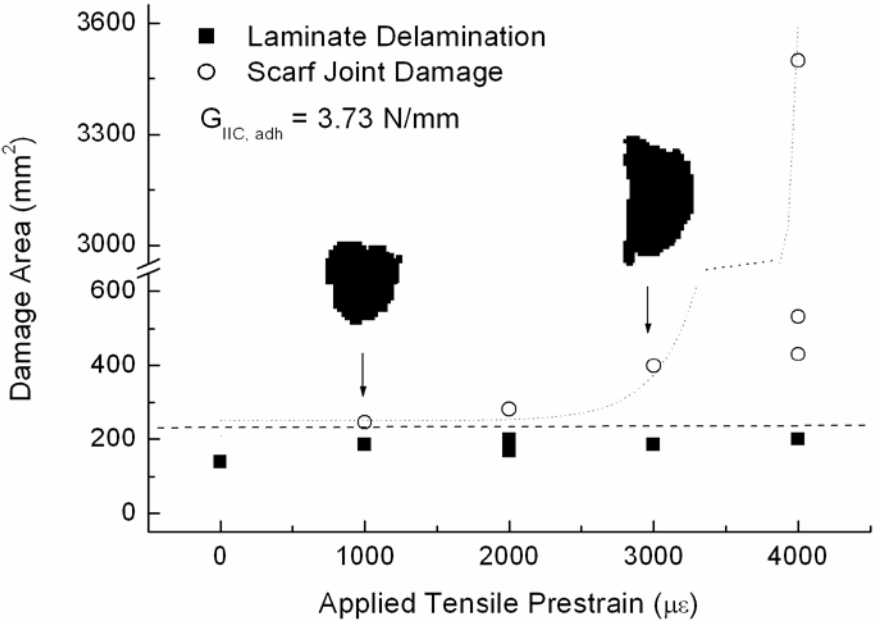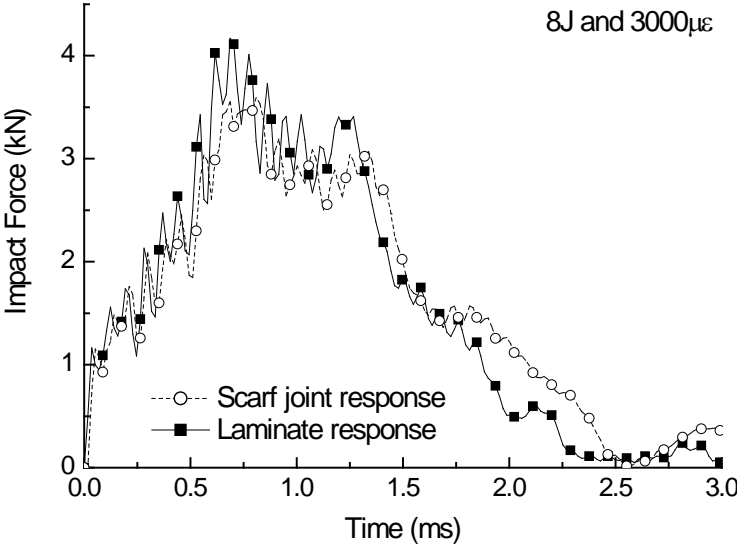

(a)
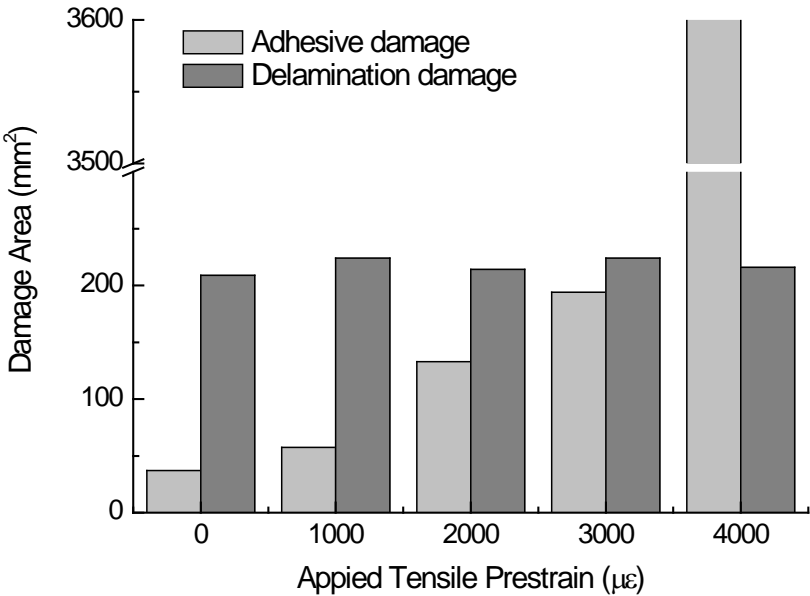
(b)

Figure 9: Comparison of force-time history for laminate coupon and scarf joint at 8J and (a) 1000με and (b) 3000με. The force-time history is insensitive to the bondline presence and adhesive damage.
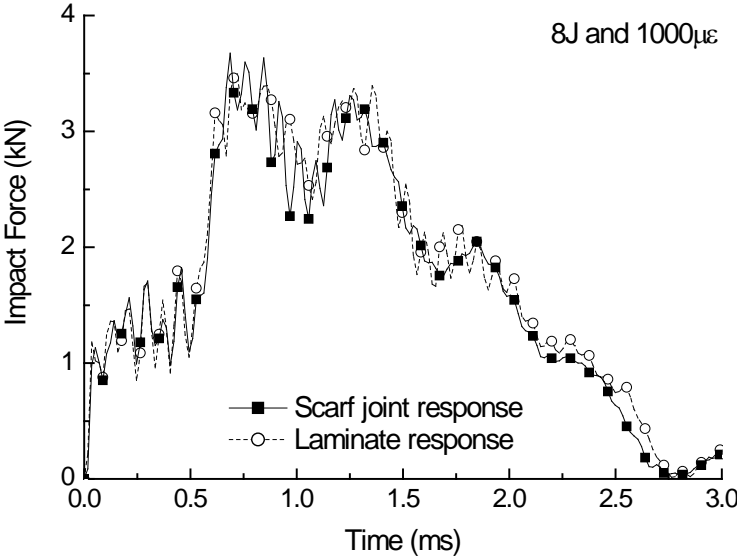
(a)

(b)

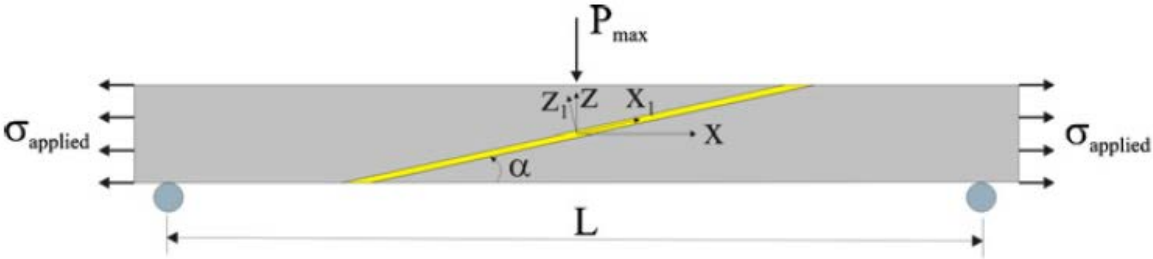Figure 10:   A scarf joint subjected to combined in-plane pre-load and impact load
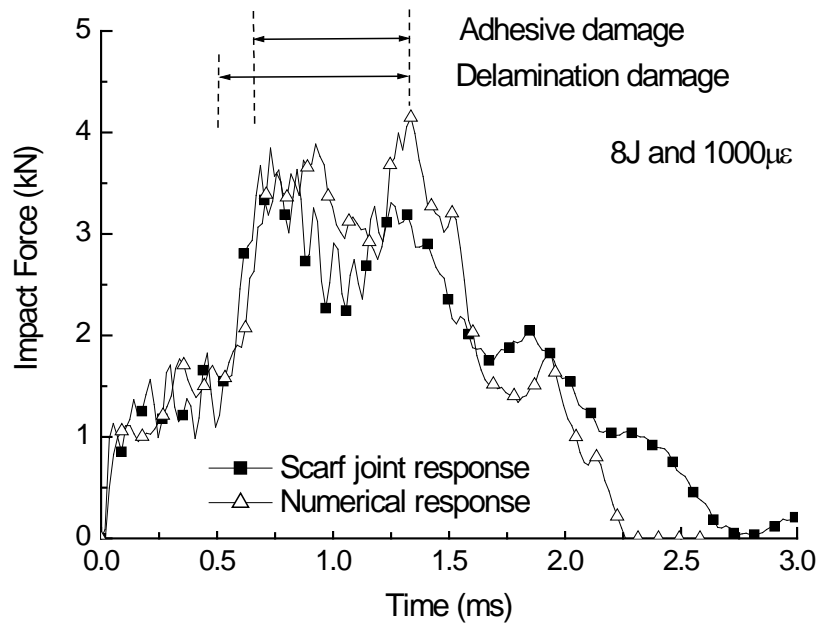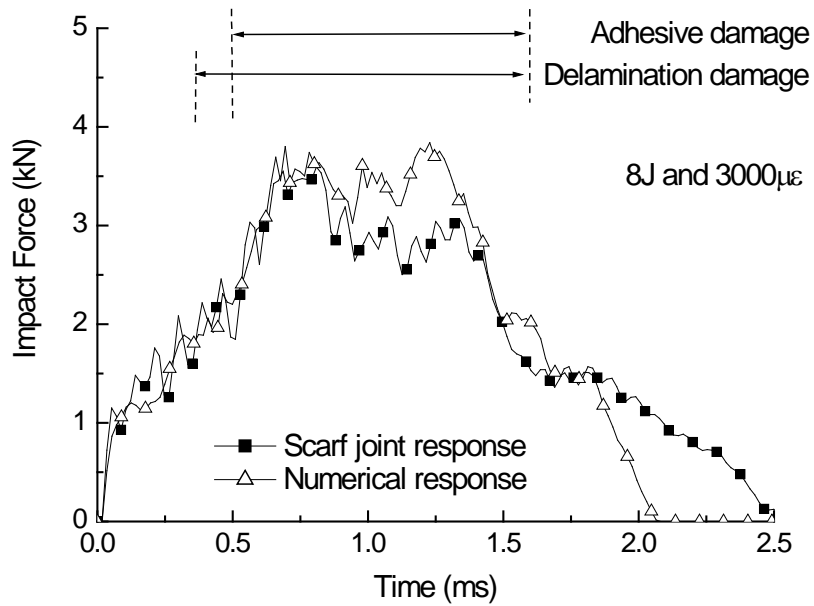
Figure 11: Comparison of experimental results with numerical predictions for scarf joint analysis and indication of damage development for (a) 1000με and (b) 3000με.

(a)

(b)

Figure 12: Damage areas for 8J and tensile pre-strain of 1000με for different damage scenarios (the total width of the adhesive layer is shown in each case): (a) adhesive damage only (no delamination), (b) delamination only (no adhesive damage), (c) combined adhesive and delamination damage, (d) side view of (c) showing bond line and delaminated area through-the-thickness.

(a) (b) (c)

(d)